HARD X-RAY INTENSITY DISTRIBUTION ALONG Hα RIBBONS

Ju Jing[1,2], Jeongwoo Lee[1], Chang Liu[1,2], Dale E. Gary[1], and Haimin Wang[1,2]

1. Physics Department, New Jersey Institute of Technology, Newark, NJ 07102

2. Big Bear Solar Observatory, 40386 North Shore Lane, Big Bear City, CA 92314

ABSTRACT

Unusual ribbon-like hard X-ray sources were found with the *Reuven Ramaty High Energy Solar Spectroscopic Imager* (*RHESSI*) observation of a 2B/M8.0 flare on 2005 May 13. We use this unique observation to investigate the spatial distribution of the hard X-ray intensity along the ribbons and compare it with the local magnetic reconnection rate and energy release rate predicted by the standard magnetic reconnection model for two ribbon flares. In the early phase of the flare, the hard X-ray sources appear to be concentrated in strong field regions within the Hα ribbons, which is explicable by the model. At and after the flare maximum phase, the hard X-ray sources become spatially extended to resemble Hα ribbons in morphology, during which the spatial distribution of hard X-ray intensity lacks a correlation with that of the local magnetic reconnection rate and energy release rate predicted by the model. We argue that the magnetic reconnection during this event may involve the rearrangement of magnetic field along the magnetic arcade axis which is inevitably overlooked by the two-dimensional model and suggest that this type of three-dimensional reconnection will be best seen in so-called sigmoid-to-arcade transformations.

Subject headings: Sun: flares — Sun: X-rays, gamma rays — UV radiation

1. INTRODUCTION

Evidence for solar magnetic reconnections comes from soft X-ray and EUV observations showing the cusp structure and growth of magnetic arcades below Coronal Mass Ejections and hard X-ray (HXR) observations of looptop and footpoint sources. In particular, Hα ribbon separation away from the magnetic polarity inversion line (PIL) has been the most solid evidence for the magnetic reconnection proceeding upward in the corona. The magnetic reconnection geometry and its evolution responsible for these features are well predicted by the so-called

CSHKP model or standard model for solar flares (Carmichael 1964; Sturrock 1966; Hirayama 1974; Kopp & Pneuman 1976; see also Priest & Forbes 2002). However it was puzzling that HXR sources are spatially much more confined than Hα ribbons, if both radiations result from the same process of the deposition of energy released in the corona into the low atmosphere. It is qualitatively conceivable that the energy difference of the particles emitting these radiations and finite sensitivities of instruments used for the observations may cause such spatial discrepancy between the HXR sources and Hα flare ribbons. Asai et al. (2002) first addressed this issue with a quantitative estimate of the energy release rate.

Asai et al.'s estimate is based on a theoretical framework of the two-dimensional (2D) magnetic reconnection discussed by Forbes & Priest (1984, the 2D model hereafter). The essence of this 2D model is that by limiting the reconnection process in the CSHKP model to the 2D slice across the PIL, a simple but quantitative expression for the electric field in the reconnecting X-point is enabled in the form: $E = u_c B_c = uB$ under the principle of magnetic flux conservation. Here, u_c is the velocity of the coronal field line coming into the X-point; B_c is the strength of that field line; B is the normal component of magnetic field; u is the transverse component of ribbon velocity. Isobe et al. (2002) applied the Poynting vector theorem to the 2D model to enable calculation of the magnetic energy release rate that is expressed as $\epsilon \sim u_c B_c^2 A$, where A is the area of the reconnecting current sheet (RCS) in the corona. Unlike the electric field that can entirely be determined by observable quantities, this energy release rate contains unknowns: B_c and A, for which two approaches have been made: one is to assume that B_c/B and A are constant during the flare (Isobe et al. 2002) and the other is to relate them to the ribbon area, again under the magnetic flux conservation principle (Lee et al. 2006). Asai et al. (2002) adopted the first approach and further argued that the inflow velocity may depend on the magnetic field as either $u_c \sim B_c^{1/2}$, for the Sweet-Parker mechanism, or $u_c \sim B_c$ for the Petschek mechanism. As a result, the energy release rate is believed to be as sensitive to the magnetic field as $\epsilon \sim B^{5/2}$ or $\epsilon \sim B^3$. For instance, spatial variation of field strength by a factor of three along the ribbon could lead to a contrast by a factor of $\sim$30 in the energy release rate. Since the dynamic range of the Yohkoh HXT is $\sim$10, the argument explains why many HXR sources tend to be in the form of highly concentrated footpoints, even at a modest contrast in field strength. However, it still leaves open the question of whether ribbon-like HXR sources may be detected using an instrument with sufficiently high dynamic range.

With the launch of the *Reuven Ramaty High Energy Solar Spectroscopic Imager* (*RHESSI*), numerous HXR sources have been observed at unprecedented dynamic range ($\leq$100, Hurford et al. 2002). Temmer et al. (2007) and Miklenic et al. (2007) revisited the problem of spatial distinction between HXR sources and Hα ribbons with RHESSI data to find that the local magnetic energy release rate in the Hα segments with and without HXR sources make a difference up to a factor of $\sim 10^2$ in their events. This result confirms the previous idea that

spatial confinement of HXR sources is due to the great sensitivity of the magnetic energy release rate to field strength (Asai et al. 2002). In contrast, ribbon-like HXR (R-HXR) sources have been found in a RHESSI observation of the 2005 May 13 flare, as opposed to more common, footpoint-like HXR (FP-HXR) sources (Liu et al. 2007). The only pre-RHESSI event that looks similar to this R-HXR event is the 2000 July 14 flare observed with the Hard X-ray Telescope on board *Yohkoh* (Masuda et al. 2001). As we noted above, qualitatively there is no problem to understand such R-HXR sources under the CSHKP model. It is, however, an unusual observation and seemingly in conflict with the above-mentioned quantitative prediction of the spatial locations of HXR sources based on the energy release rate calculated under the 2D model. To have an R-HXR source under the 2D model, the magnetic energy release in the corona should be homogeneous, and as a consequence the footpoint magnetic field and its motion should also appear nearly uniform in all parts of the ribbons. In this Letter, we investigate the HXR intensity and magnetic field distribution along the Hα ribbon in the 2005 May 13 event and discuss whether this new phenomenon of R-HXR sources can still be understood in terms of the 2D reconnection model.

2. Data Analysis

The 2B/M8.0 flare of 2005 May 13 occurred in active region NOAA 10759, with the maximum HXR emission at 16:42 UT. We use the same RHESSI HXR maps as constructed in Liu et al. (2007) which are from the photons integrated for six time intervals: five one-minute intervals (*a*–*e*) from 16:39:34 to 16:44:34 plus one interval *f* from 16:44:56 to 16:45:56 (see Fig. 1 of Liu et al. 2007). Grids 1–9 were used. The CLEAN algorithm with natural weighting was used to find the ribbon-like HXR sources. We add the Hα observation obtained from the Optical Solar Patrol Network (OSPAN; formerly known as ISOON) that has 1 arcsec pixel resolution and 1 minute cadence. A co-aligned magnetogram obtained with Michelson Doppler Imager (MDI) is used to approximately measure the normal component of the magnetic field B, as the active region was near the disk center (N12E05).

Figure 1 shows the HXR sources and ribbon locations at two selected times on top of Hα images and the MDI magnetogram. The left and middle panels show HXR (red contours) on top of the inverse OSPAN Hα images (grayscale) taken at 16:40:11 UT and 16:44:03 UT, respectively. The HXR maps represent intensity integrated in the time intervals *a* (16:39:34 - 16:40:34 UT) and *e* (16:43:34 - 16:44:34 UT) in the 25-50 keV energy range. Note also that the contours in both panels are in the same absolute levels (0.075, 0,085, 0.095, 0.105 and 0.115 photons cm^{-2} s^{-1} arcsec^{-2}) so that the appearance of the FP-HXR or R-HXR sources is independent of the choice of contour level. The symbol connected lines are the multiple

locations along the ribbons determined by finding the local maximum Hα intensity along the direction perpendicular to the magnetic PIL. In the left panel, the HXR sources were typical, compact FP-HXR sources lying within the Hα ribbons, while in the middle panel, the HXR sources have elongated to fill the eastern ribbon area more or less uniformly. Since both HXR sources are plotted in the same contour levels, the R-HXR in the middle panel is not due to the relative decrease of the overall intensity, but due to appearance of the new sources in regions off from the initial FP-sources. As discussed in the previous paper (Liu et al. 2007), the increase in R-HXR area in the later phase is not an instrumental or observational effect but an intrinsic feature of the HXR emission. The rightmost panel shows the flare ribbon axes read from Figure 1*ab*, on top of the co-aligned magnetogram taken at 16:03:30 UT. The blue lines are the PILs. The displacement of the ribbon location is measured using the index j coordinates determined at each time (displayed in Figure 1) as a tracer of the motion. We also selected nine positions (red dots numbered from 1 to 9 along the eastern ribbon) to investigate their temporal evolution of HXR intensity for later use.

After we determine u and B as a function of position and time, we use them to construct uB and uB^2 in comparison with the HXR intensity distribution along the ribbon axis. According to the 2D model, uB is equivalent to the electric field or local reconnection rate, but uB^2 serves as a proxy of the energy release rate subject to the assumption that A and B_c/B do not vary with time. This assumption may not be valid in general but is unlikely to be an important factor in our current study of the spatial correlation, since these quantities do not vary significantly with position along the ribbon. Figure 2 shows the 25-50 keV HXR intensity I_{HXR}, the electric field uB, and the proxy of energy release rate uB^2 with the red, green and blue curves, respectively, corresponding to the six time intervals *a*–*f*. They are shown as functions of position within the ribbon, given in terms of the index coordinates for the points displayed in Figure 1. The scale of each quantity is specified, and kept the same for all panels so that we can see the lightcurves at six time intervals if time behavior is of interest. In the early phase (panels *a*-*c*) there are two FP-HXR sources located in regions with strong magnetic field. The best correlation is seen in panel *c*, which indeed gives strong support for the model prediction of energy release rate. After the flare maximum phase (panel *c*), the elongated R-HXR sources show up, lacking spatial correlation with the magnetic field (panels *d* and *e*). While the former property agrees with the 2D model, the latter is in conflict with the 2D model.

Finally, we examine the time evolution of I_{HXR} at given positions within the ribbons. In principle, this can be seen by looking the relative time-variations at fixed j coordinates in Figure 2. For better clarity, however, we plot in Figure 3 the spatially-resolved lightcurves of HXR intensity at the nine selected positions (red dots in Fig. 1). The HXR intensity at positions of initially FP type (2, 6, 5) reaches maximum at the flare peak time and then decreases after the peak time. On the other hand, the HXR intensity at other positions off from the FP-HXR

sources (3, 7, 9) continue to increase after the flare peak time, and reaches maximum later. This relative time difference of the peaks at different positions leads to the appearance of the R-HXR in the late phase. In other words, the appearance of the R-HXR sources in the late phase (*d*-*e*-*f* in Figure 2) is not merely due to the relative weakening of the FP-HXR sources, but a result of new appearance or enhancement of the HXR intensity in regions off from the initial FP-HXR sources. This behavior is unseen in other typical HXR events in which off-peak region sources remain dim and do not evolve to R-HXR sources while FP-sources come up and fade away during the flare.

3. DISCUSSION

With the unusual R-HXR sources observed with RHESSI on 2005 May 13, we are able to compare the spatial distribution of the HXR intensity along the ribbon axis with those of the local reconnection rate $E = uB$ and a proxy for magnetic energy release rate $\epsilon \sim uB^2$ in the corona as predicted under the 2D model for magnetic reconnection. In our result, the HXR intensity distribution shows a good spatial correlation with the reconnection rate or energy release rate in the early phase, but the HXR intensity distribution becomes more uniform in the late phase, lacking a correlation with those quantities. With this result we conclude that the R-HXR phenomenon is not explained by the 2D model, whereas the FP-HXR sources in early phase are indeed explained by the 2D model.

Since theoretical tools for quantitative interpretation of ribbon observations under three-dimensional (3D) reconnection are yet to developed (Hesse et al. 2005, Isenberg & Forbes 2007), we attempt to only qualitatively describe how 3D reconnection will help for explanation of the present observation with cartoons plotted in Figure 4. Note that in this cartoon, only a few field lines are shown for purposes of illustration, but field lines exist everywhere above the ribbons. Those sections where we do not explicitly show field lines have weaker fields and correspondingly smaller amounts of energy release which is, however, enough to form Hα ribbons. We now focus on the formation of HXR sources only.

Figure 4*a* shows a scenario in which a magnetic arcade is a stack of 2D structures which are independent of each other. Initially the ribbon sections with stronger magnetic field strength are connected to the coronal parts with correspondingly stronger coronal fields (black lines). When the reconnection occurs, they become the FP-HXR sources as they receive the energy deposition at a higher rate. At a later time (gray lines), the reconnecting X-line moves to a higher coronal height, where similar magnetic field inhomogeneity exists, and energy release rate at this time is again spatially inhomogeneous to produce FP-HXR sources in the surface. Since many HXR observations have shown FP sources in motion, this simplistic approach of

representing a 3D arcade with a stack of 2D loops (including those topologically equivalent to 2D loops) should, in fact, be considered adequate for explaining the majority of HXR sources.

The alternative scenario, shown in Figure 4*b*, is same as the above one in the early phase (black lines), but undergoes a different evolution in the later phase (gray lines). In this case, the magnetic reconnection results not only in a change of the magnetic topology but also magnetic flux exchange to rearrange the distribution of the coronal magnetic field along the direction of arcade axis. As a result, the energy release rate will also redistribute along the X-line at its new height. On the other hand, magnetic field lines are still tied to the photosphere where they are distributed inhomogeneously. Therefore the renewed coronal distribution of the energy release rate may not exactly reproduce itself in the photosphere, but may smooth the FP-HXR sources out to some extent to produce R-HXR sources. We call this a 3D reconnection in the sense that it involves a magnetic field evolution in the third dimension unspecified by the 2D model. Since R-HXR sources are rarely observed, this type of 3D reconnection should require a special condition for its occurrence.

As a plausible configuration that can lead to the second scenario, we recall that the source active region of this 2005 May 13 event was a sigmoid active region and underwent so-called the sigmoid-to-arcade transformation during the flare (Liu et al. 2007). The sigmoid-to-arcade transformation is an exclusive phenomenon (Sterling et al. 2000) interpreted as due to reconnection that occurs in two inner legs of the sigmoidal field lines and progressively continues into the legs of the envelope field to form an arcade (Moore et al. 2001). It is conceivable that this type of magnetic reconnection is 3D in current context, since it involves not only the magnetic topology change above each arcade loop but also a field redistribution along the arcade axis (Manchester et al. 2004). We conclude that the R-HXR phenomenon is a signature of a type of 3D reconnection, and that sigmoid active regions are probably a strong candidate for producing the rare R-HXR phenomenon and the associated 3D magnetic reconnection. It is thus considered worthwhile to extend the current study to other RHESSI observations of sigmoid active regions. Such a study is underway.

We thank the referee for the helpful comments. We thank *RHESSI* team for excellent data set. JJ, CL and HW were supported by NSF under grant ATM-0536921 and ATM-0548952 and NASA under grant NNX0-7AH78G. JL and DG were supported by NSF grant AST 06-07544 and NASA grant NNG0-6GE76G.

REFERENCES

Asai, A., Masuda, S., Yokoyama, T., Shimojo, M., Isobe, H., Kurokawa, H., & Shibata, K., 2002, ApJ, 578, L91

Carmichael, H., 1964, in The Physics of Solar Flares, ed. W. N. Hess (NASA SP-50; Washington, DC:NASA), 451

Fletcher, L., Pollock, J. A., & Potts, H. E. 2004, Sol. Phys., 222, 279

Forbes, T.G. and Priest, E.R.: 1984, in Solar Terrestrial Physics: Present and Future, ed. D.M. Butler, K. Papadopoulous (NASA RP-1120, Washington, D.C.) p 1

Hesse, M., Forbes, T. G., & Birn, J., 2005, ApJ, 631, 1227

Hirayama, T., 1974, Sol. Phys., 187, 229

Hurford, G. J., 2002, Sol. Phys., 210, 61

Isenberg, P. A. & Forbes, T. G., 2007, ApJ, submitted

Isobe, H., Yokoyama, T., Shimojo, M., Morimoto, T., Kozu, H., Eto, S., Narukage, N., & Shibata, K., 2002, ApJ, 566, 528

Kopp, R. A., & Pneuman, G. W., 1976, Sol. Phys., 50, 85

Lee, J., Gary, D. E., & Choe, G. S., 2006, ApJ, 647, 638

Liu, C., Lee, J., Gary, D. E., & Wang, H., 2007, ApJ, 658, L127

Masuda, S., Kosugi, T., & Hudson, H. S., 2001, Sol. Phys., 204, 55

Manchester, W., IV, Gombosi, T., DeZeeuw, D., & Fan, Y., V., 2004, ApJ, 610, 588

Miklenic, C. H., Veronig, A. M., Vršnak, B., & Hanslmeier, A., 2007, A&A, 461, 697

Moore, R. L., Sterling, A. C., Hudson, H. S., & Lemen, J. R., 2001, ApJ, 552, 833

Priest, E. R. & Forbes, T. G. 2002, A&ARv, 10, 313

Sterling, A. C., Hudson, H. S., Thompson, B. J. & Zarro, D. M., 2000,ApJ, 532, 628

Sturrock, P. A. 1966, Nature, 221, 695

Temmer, M., Veronig, A. M., Vršnak, B., & Miklenic, C., 2007, ApJ, 654, 674

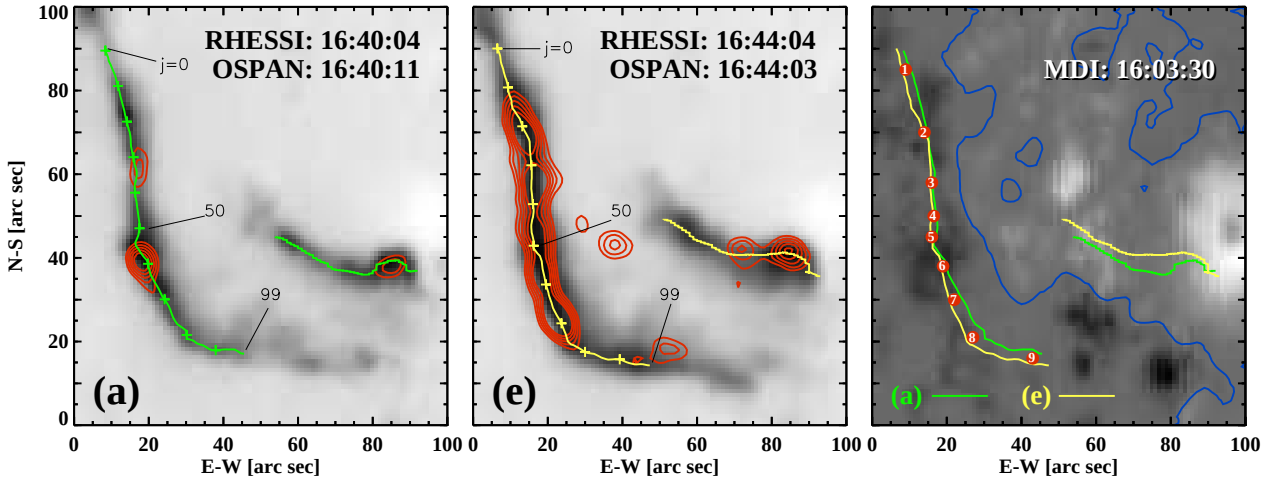

Fig. 1.— Left and Middle: the inverse OSPAN Hα images taken at 16:40:11 UT and 16:44:03 UT, respectively. The red contours show HXR intensity integrated in the time intervals *a* (16:39:34 - 16:40:34 UT) and *e* (16:43:34 - 16:44:34 UT), from RHESSI data in the 25-50 keV energy range. The contour levels are 0.075, 0,085, 0.095, 0.105 and 0.115 photons cm^{-2} s^{-1} arcsec^{-2}, respectively. The symbol connected lines show locations of Hα ribbons. Right: the MDI magnetogram taken at 16:03:30 UT. The blue lines show the magnetic polarity inversion line, and the green and yellow lines show the ribbon locations displayed in the left two panels. Red dots numbered from 1 to 9 mark the nine positions along the eastern ribbon, which are used in Figure 3.

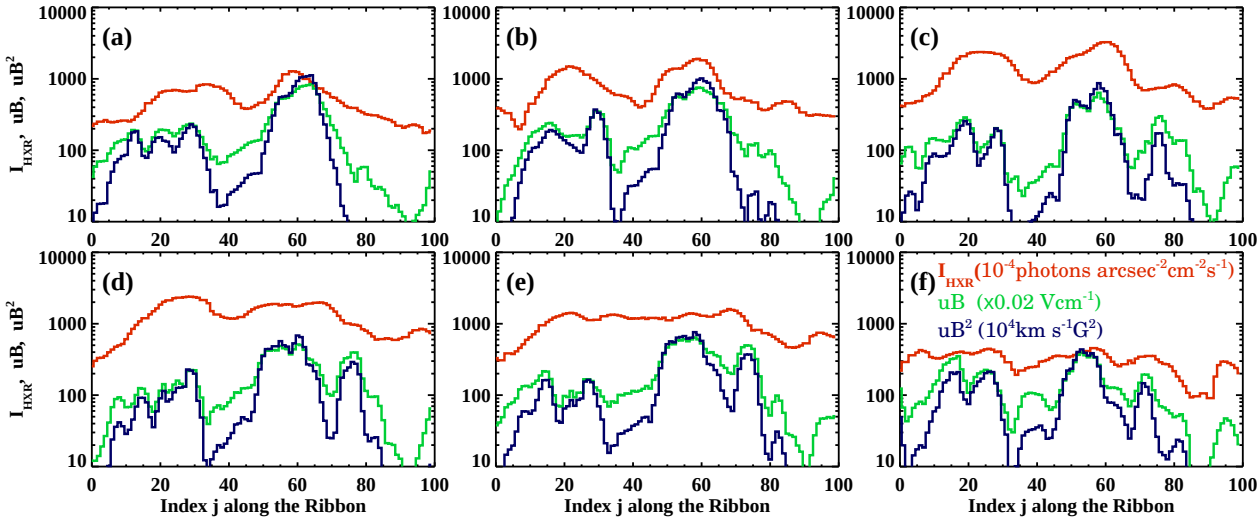

Fig. 2.— The spatial distribution of HXR intensity (red) in comparison with that of uB (green) and uB^2 (blue), shown as functions of the ribbon distance index defined in Figure 1. Panels (a) to (f) correspond to the six 1-min time intervals used to create the 25-50 keV RHESSI images.

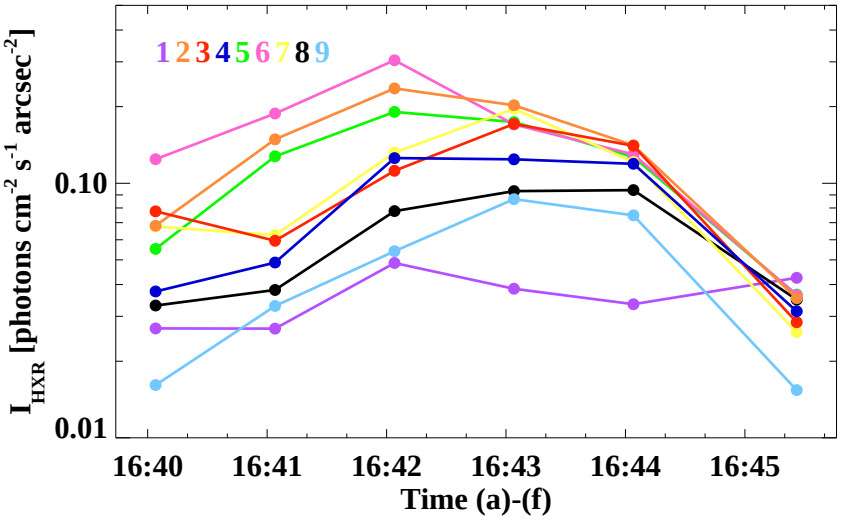

Fig. 3.— The temporal variations of the HXR intensity at the nine positions that are marked by the dots in Figure 1.

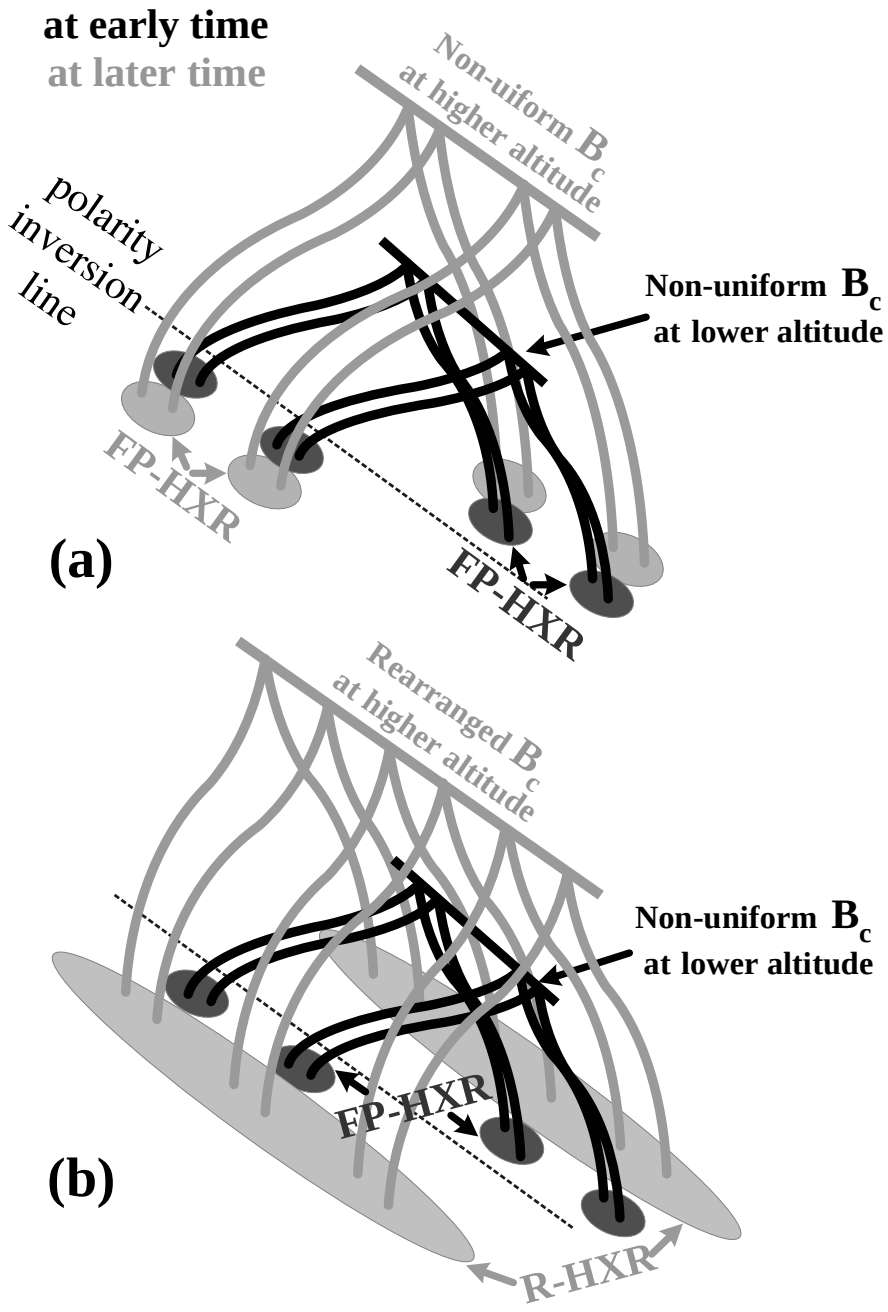

Fig. 4.— Cartoons of two distinct scenarios for explaining (a) FP-HXR sources and (b) R-HXR sources. For illustration, we plot only a few field lines, but field lines exist everywhere, and the spacing between the plotted field lines implies the relative strength of the magnetic field. Field lines in an early phase are shown as black lines, and those at later phase in gray lines.